

The catalytic effect of boron substitution in MCM-41-type molecular sieves

V. Sundaramurthy, I. Eswaramoorthi, and N. Lingappan

Abstract: A series of B-MCM-41 samples has been synthesized with a wide range of boron content ($\text{SiO}_2\text{:B}_2\text{O}_3$ ratio from 20 to 200), using ethyl silicate ester-40 (ES-40) as the silica source and characterized by XRD, BET, FT-IR, ^{11}B -MAS NMR, SEM, pyridine adsorption, TPDA, and chemical analysis. The interplanar d_{100} spacing varies from 40 to 45 Å, depending on the Si:B ratio. On calcination, a significant amount of four-coordinated boron is converted into less stable three-coordinated boron, and some boron is removed from the framework. The degree of deboronation increases with an increase of boron content of the sample. The B substitution in the MCM-41 framework results in only weak and mild acid sites. The isomerization of 1-hexene is found to be influenced by the boron content in the framework. The isomerization leads to both a hydrogen shift and skeletal rearrangement. The selectivity ratios of *cis*-2-hexene to *trans*-2-hexene and 2-hexene to 3-hexene were found to decrease with an increase of temperature and a decrease of the $\text{SiO}_2\text{:B}_2\text{O}_3$ ratio of the catalysts. Skeletal isomerization starts at 250 °C, forming secondary products, and increases with an increase of temperature and an increase of boron content of the catalysts.

Key words: ES-40, B-MCM-41, deboronation, catalyst characterization, XRD, BET, FT-IR, ^{11}B -MAS NMR, SEM, 1-hexene isomerization, 2-hexene.

Résumé : Utilisant l'ester silicate d'éthyle-40 (ES-40) comme source de silicium, on a synthétisé une série d'échantillons B-MCM-41 comportant des quantités très variables de bore (rapport $\text{SiO}_2\text{:B}_2\text{O}_3$ allant de 20 à 200) qu'on a caractérisé par analyse chimique ainsi que par XRD, BET, FT-IR, RMN du ^{11}B -MAS, SEM, adsorption de la pyridine et TPDA. L'espace interplanaire d_{100} varie de 40 à 45 Å suivant la valeur du rapport Si:B. Par calcination, une quantité importante de bore tétracoordiné est transformée en bore tricoordiné et moins stable et une certaine quantité de bore est éliminée du squelette. Le degré de déboronation augmente avec une augmentation dans la teneur en bore de l'échantillon. La substitution du bore dans les échantillons de MCM-41 ne conduit qu'à des sites acides faibles et doux. On a observé que l'isomérisation de l'hex-1-ène est influencée par la teneur en bore du squelette. L'isomérisation conduit à des migrations d'hydrogène et à des réarrangements du squelette. On a observé que les rapports de sélectivité *cis*-hex-2-ène:*trans*-hex-2-ène et de hex-2-ène:hex-3-ène diminuent avec une augmentation de la température et une diminution du rapport $\text{SiO}_2\text{:B}_2\text{O}_3$ des catalyseurs. L'isomérisation du squelette commence à 250 °C avec formation de produits secondaires et elle augmente avec la température et avec une augmentation dans la teneur en bore des catalyseurs.

Mots clés : ES-40, B-MCM-41, déboronation, caractérisation du catalyseur, XRD, BET, FT-IR, RMN, ^{11}B -MAS, SEM, isomérisation du hex-1-ène, hex-2-ène.

[Traduit par la Rédaction]

Introduction

MCM-41 is a novel mesoporous material first described by Kresge et al. (1) in 1992. MCM-41 possesses unidirectional channel-like pores of uniform size, which are arranged in a regular hexagonal pattern. The pore diameters are adjustable in the range 15–100 Å, depending on the synthesis conditions, such as temperature, type, and size of the templating detergent cations. Current research on MCM-41 has two major aims. One is to find cheaper raw materials for synthesis. The other aim is to modify the framework of

MCM-41, to generate catalytic sites needed for different types of reactions. Isomorphous substitution of Al (2–8), Ti (9, 10), Ga (11), and V (12, 13) in the MCM-41 framework has been described in the literature. The incorporation of boron in the MCM-41 structure has been claimed since 1994 (14). Definite evidence for boron in the MCM-41 framework position (14–23) and MCM-48 framework position (23) has been provided using various techniques. The growing interest in the synthesis of borosilicates is because they could be useful for synthesizing other metallosilicate analogues, which are sometimes difficult to synthesize by direct hydro-

Received 18 November 2002. Published on the NRC Research Press Web site at <http://canjchem@nrc.ca> on 6 May 2004.

V. Sundaramurthy,^{1,2} I. Eswaramoorthi, and N. Lingappan. Department of Chemistry, Anna University, Chennai-25, India.

¹Present address: Laboratoire Catalyse Spectrochimie (LCS), UMR CNRS 6506, ENSICAEN, 6, boulevard Maréchal Juin, 14050, Caen CEDEX, France.

²Corresponding author (e-mail: sundaramurthyved@hotmail.com).

thermal methods (24, 25). Mixtures of silica sources such as Cab-O-Sil M5 fumed silica, sodium silicate, and tetramethylammonium silicate (17), Cab-O-Sil M5 fumed silica and sodium silicate (19), and Ludox and sodium silicate (15) were used to synthesize B-MCM-41. Oberhagemann et al. (22) used a single silica source, tetramethoxysilane. The synthesis of B-MCM-41 using ethyl silicate-40 (ES-40) has not been studied so far. ES-40 is an oligomer silica with a molecular formula of $(\text{C}_2\text{H}_5\text{O})_3\text{Si}[\text{O}-\text{Si}(\text{OC}_2\text{H}_5)_2]_3\text{O}-\text{Si}(\text{OC}_2\text{H}_5)_3$. It is a transparent liquid containing 40% silica (SiO_2) by mass. ES-40 is perfect for industrial use, considering the efficiency with which it supplies silica and its viscosity, specific gravity, stability when stored, and ease of handling during use. With its high silica content and cost, which has been kept low, ES-40 is widely used in industrial applications. We have already reported the synthesis of B-ZSM-5 using ES-40 as the silica source (26). Dongare and co-workers (27) and Mrowiec-Bialon and Jarzebski (28) reported synthesis of titanium silicalite-1 and sol-gel composites using ES-40.

The protonic form of borosilicate molecular sieves is less acidic than their aluminosilicate counterparts because of a lack of strong Brønsted acidity. Hence, the catalytic properties of borosilicate zeolites, especially B-ZSM-5, are being used for less acidity-demanding reactions such as double-bond migration in olefins (26, 29, 30), dehydration of aldehydes (31), *N*-methylaniline synthesis from aniline (32), and Beckmann rearrangement of cyclohexanone oxime to caprolactam (33). The weakly acidic sites in B-MCM-41 are reported to show high selectivity of isoprene by Prins condensation of isobutylene with formaldehyde (34). In the literature no report is available in detail on B-MCM-41 catalytic activity, particularly in hexene isomerization. Pines and Haag (35), Brouwer (36), and West et al. (37) used 1-hexene isomerization as a catalytic test for the evaluation of the relative acidity of alumina, silica alumina, and silica gel, respectively. The reports are available on 1-hexene isomerization over HY (38) and ZSM-5 zeolite (39, 40). Gati and Resofszki (41) and Paal et al. (42) studied double-bond isomerization over metal oxides and EUROPT-1, respectively. Zhiping and Changqing (43) studied the same reaction over phosphatotungstic acid catalyst. In this paper, we describe the synthesis of B-MCM-41 using ES-40, characterization of this molecular sieve by physico-chemical techniques, and its catalytic activity in 1-hexene isomerization. Further, the significant differences between the catalytic effects of B-MCM-41 and Al-MCM-41 were studied, and the ratio of selectivity of 2-hexenes was compared with those previously obtained (26) for B-ZSM-5 under similar conditions.

Experimental

Synthesis

Materials used were ethyl silicate-40 (ES-40, 40% SiO_2) (Mettur Chemicals, South India), sodium aluminate (AR), boric acid (Baker), cetyltrimethylammonium bromide (CTAB) (Ottokemi), sodium hydroxide (E. Merck), sulphuric acid (AR), and demineralized water.

A series of boron-containing MCM-41 samples were synthesized hydrothermally, using gel with the following molar

composition: $\text{SiO}_2 : 0.19 \text{ Na}_2\text{O} : 0.25 \text{ CTAB} : 63 \text{ H}_2\text{O} : x \text{ B}_2\text{O}_3$.

The $\text{SiO}_2:\text{B}_2\text{O}_3$ ratio (i.e., 1: x) was varied from 20 to 200. The following is the experimental procedure adopted in the preparation of a sample with an $\text{SiO}_2:\text{B}_2\text{O}_3$ ratio of 50, as a typical case.

Diluted H_2SO_4 (30 mL water containing 0.5 mL concd. H_2SO_4) was added to ethyl silicate ester (20 g) and stirred mechanically. After 1 h, a solution of 12 g of CTAB in 50 mL of water was added to the previous silica-water slurry. After another 15 min, 20 mL of an aqueous solution containing 0.34 g of H_3BO_3 was added. Subsequently, a solution of sodium hydroxide (2 g in 50 mL water) was added carefully, to get a gel at pH 11. The gel obtained was transferred into a 300-mL stainless steel autoclave, and the sealed autoclave was heated statically in an air oven at 120 °C for 10 days. The crystallized mass was filtered, thoroughly washed, and then dried in static air at 120 °C. The solid product, which weighed about 7.0 g, constituted 87% yield on the basis of SiO_2 . By varying the $\text{SiO}_2:\text{B}_2\text{O}_3$ ratio in the initial gel to 20, 50, 100, and 200, samples B-1, B-2, B-3, and B-4, respectively, were synthesized at 120 °C. The Al-MCM-41 (sample A-1) with gel $\text{SiO}_2:\text{Al}_2\text{O}_3 = 20$ was synthesized from a gel of molar composition $\text{SiO}_2 : 0.19 \text{ Na}_2\text{O} : 0.25 \text{ CTAB} : 63 \text{ H}_2\text{O} : 0.05 \text{ Al}_2\text{O}_3$, following the experimental procedure described above for B-MCM-41 but with H_3BO_3 replaced by sodium aluminate (2.4 g). Siliceous MCM-41 was crystallized using the same procedure but with no boron or aluminum. The organic cations in the channels were removed by calcination of samples under flowing dry nitrogen with a raise in temperature to 550 °C at a rate of 5 °C min^{-1} . The temperature was kept constant at 550 °C for 2 h before switching over slowly from N_2 to dry air. After an additional 4 h at 550 °C, the samples were cooled to room temperature under flowing air and stored in a desiccator. The calcinated samples were exchanged with a 1 mol L^{-1} solution of NH_4Cl (50 mL g^{-1} sample) at 80 °C for 10 h. The samples were filtered, washed with hot water, and dried at 120 °C. The procedure was repeated two more times to obtain maximum exchange. The acidic or protonated form of the catalyst was obtained by calcination of the NH_4 form of the sample at 550 °C, with a raise in temperature as described earlier.

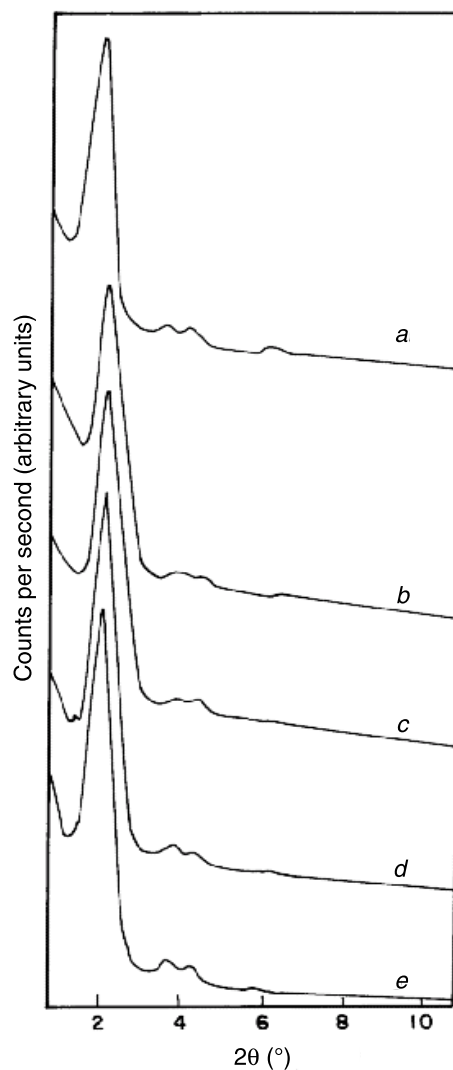
Characterization

The powder X-ray diffraction patterns of samples were recorded on a Rigaku X-ray diffractometer in the scan range of 2θ between 1° and 10°, using Cu-Ni 40-kV/30-mA radiation. The unit cell parameter (a_0) was calculated using the formula $a_0 = 2d_{100}/\sqrt{3}$. The IR spectra of the samples were recorded on a Testscan Shimadzu FT-IR 8000 series FT-IR spectrophotometer using KBr pellets. Each IR spectrum was recorded in the range 2000–250 cm^{-1} . Boron-11 magic angle spinning (MAS) NMR spectra were recorded on a Bruker Avance 400 spectrometer operating at 128.33 MHz. The zirconia rotor (7 mm o.d.) was spun at 6 kHz about the magic angle. The spectra were obtained with a $\pi/2$ pulse duration of 2.3 μs and a repetition time of 1.8 s. To prevent rehydration, the dehydrated protonated B-MCM-41 sample was transferred into the NMR rotor in a glove box under dry nitrogen gas. Chemical shifts were determined relative to

$\text{BF}_3 \cdot \text{O}(\text{C}_2\text{H}_5)_2$. The morphology of samples was investigated using scanning electron microscopy (Leica, Stereoscan). The samples were suspended in acetone, and the specimen stub was dipped into the liquid and removed. The powder got deposited onto the surface of the stub evenly when the acetone evaporated. This specimen was coated with an Au–Pd evaporated film to prevent sample charging. Surface area measurements were carried out in a Sorptometric 1990 CE instrument following the BET procedure, using nitrogen as the adsorbent at liquid nitrogen temperatures. Prior to adsorption, the calcinated samples were degassed at 200 °C for 15 h under pressure. Helium was the carrier gas and a thermal conductivity detector was used. The molar compositions of the samples were obtained by wet chemical analysis. Silica in each sample was determined by taking the weight loss after treatment with hydrofluoric acid. Quantitative estimations of boron and sodium were done using inductively coupled plasma atomic emission spectrometry (ICPAES). The organic cation and water contents in the samples were determined by weight loss in TGA (Mettler TA 3000). FT-IR spectra of chemisorbed pyridine was recorded using a specially designed, all-silica, in situ controlled-environment cell. The samples were activated under vacuum (10^{-6} torr (1 torr = 133.322 Pa)) at 400 °C for 5 h and then cooled to 100 °C. Then the samples were allowed to adsorb pyridine for 1 h. Excess and physisorbed pyridine was removed by evacuation for 1 h before the spectra were recorded at 100 °C. Similarly, the pyridine-adsorbed samples were heated to 150, 200, and 250 °C successively under vacuum for 1 h at each temperature before the spectra were recorded. For the studies of temperature-programmed desorption of ammonia (TPDA), samples in H-form were activated at 500 °C for 1 h in a flow of He and then cooled to 120 °C in an He atmosphere; then, ammonia was sorbed at 120 °C. The He flow rate was increased to 40 mL min⁻¹ for 1 h to remove the physically adsorbed ammonia. Thermal desorption was carried out in a stream of dry He at a heating rate of 10 °C min⁻¹. The desorbed amount of NH₃ was recorded continuously using a thermal conductivity cell.

The catalytic runs were carried out in a fixed-bed down-flow reactor in the temperature range 200–350 °C. The H-form of the catalyst of particle size 20–40 mesh was kept in the middle of the reactor and was activated in pure dry air at 550 °C for 4 h, and the reaction temperature was brought down. The feed (1-hexene of 97.78% purity (Fluka)) was passed at a liquid hourly space velocity (LHSV) of 3 h⁻¹. The products were analyzed by a Hewlett-Packard 5890 A gas chromatograph. Identification of products was facilitated by use of a Finnigan MAT MS automated GC mass spectrometer. At the end of the reaction run, the reactor was flushed with nitrogen to remove the adsorbed hydrocarbons. A portion of the catalyst was removed, and the coke deposited on the catalyst was estimated from the weight loss in TGA (Mettler TA 3000). In this study, about 20–30 mg of the spent catalyst sample was subjected to temperature-programmed TGA (20 °C min⁻¹). The heating was done from ambient temperature to 800 °C in the presence of an air stream with a flow rate of 25 mL min⁻¹. A correction was made for weight loss due to moisture in the sample from the temperature profile (the weight loss from room temperature to 250 °C being ascribed to moisture). The low-temperature

Fig. 1. X-ray diffraction patterns of the synthesized Al-MCM-41 and B-MCM-41: (a) A-1; (b) B-1; (c) B-2; (d) B-3; (e) B-4.



(250–500 °C) TGA weight loss corresponds to soft coke, whereas the high-temperature (500–800 °C) weight loss is attributed to hard coke molecules (44).

Results and discussion

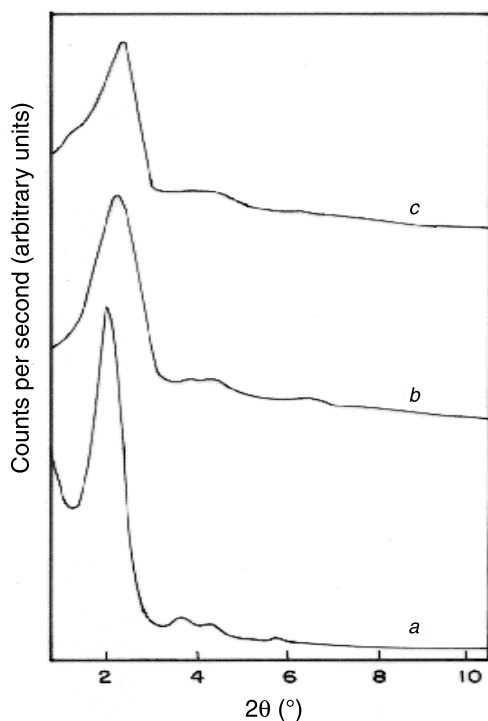
X-ray diffraction

The X-ray diffraction patterns of the synthesized B-1 to B-4 and A-1 samples shown in Fig. 1 match well with that of the boron-free silicious MCM-41 and also with the patterns reported by Sayari et al. (17) and Oberhagemann et al. (14) for B-MCM-41 and that of Kresge et al. (2) for Al-MCM-41. One major peak, at $2\theta = 2.0^\circ$, along with three peaks at $2\theta = 3.7^\circ$, 4.2° , and 6.0° are observed for all the five samples. Beck et al. (3) indexed these peaks for a hexagonal unit cell. The unit cell parameter (a_0) and d_{100} spacing are given in Table 1. Thus, it is observed that the a_0 and d_{100} spacing decrease with an increase of the boron content of the synthesized samples (B-4 to B-1). Further, the decrease in the a_0 and d_{100} spacings of B-MCM-41, as compared with its pure silica analogue, is evidence for the boron in the sili-

Table 1. The unit cell parameter (a_0), d_{100} spacing, pore diameter, and pore volume of M-MCM-41 samples (M = B, Al, and Si).

Sample	d_{100} spacing (Å)	a_0 (Å)	Pore diameter (Å)	Pore volume ($\text{cm}^3 \text{g}^{-1}$)
B-1	40.5	46.7	29.2	1.02
B-2	42.3	48.8	30.3	1.16
B-3	43.8	50.6	31.0	1.06
B-4	44.7	51.6	31.6	0.92
Si-MCM-41	45.9	53.0	31.9	1.08
A-1	48.5	56.0	32.7	1.15

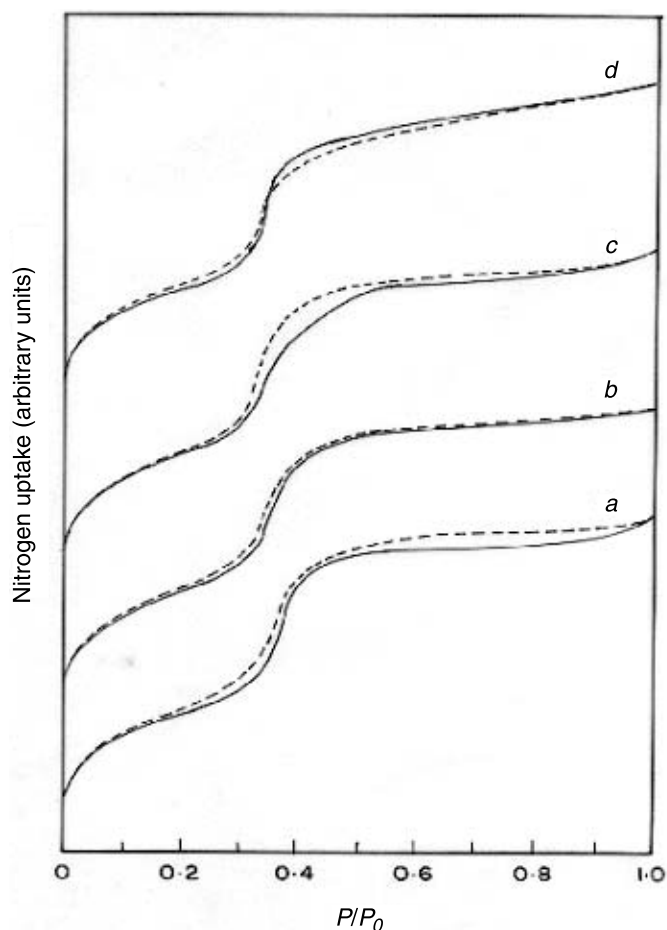
Fig. 2. X-ray diffraction patterns of the (a) synthesized, (b) calcinated Na-form, and (c) H-form of B-1.



cate framework. This is akin to the observation of Liu et al. (19) in their B-MCM-41 study, where a decrease in the d_{100} value with an increase of the boron content was observed. The increasing d spacing for the Al-MCM-41, compared, on similar lines, with Si-MCM-41, indicated that Al was incorporated into the framework.

The stability of the MCM-41 structure after removal of the template and conversion into the protonated form has also been studied using XRD. The X-ray diffraction patterns of the synthesized, calcinated, and protonated forms of a typical sample B-1 are shown in Fig. 2. On calcination (to remove the template), the peak at $2\theta = 2^\circ$ becomes weaker and broader than that of the synthesized sample. On further conversion to the ammonium form and then to the hydrogen form, the intensity of the peak decreases slightly, and the peak becomes significantly broader than that of the calcinated form. The observed changes are attributed to the increasing formation of nonstructural B and the accompanying collapse of a portion of the borosilicate framework.

Fig. 3. N_2 isotherms of B-MCM-41 samples: (a) B-1; (b) B-2; (c) B-3; (d) B-4; (—) adsorption; (- - -) desorption.

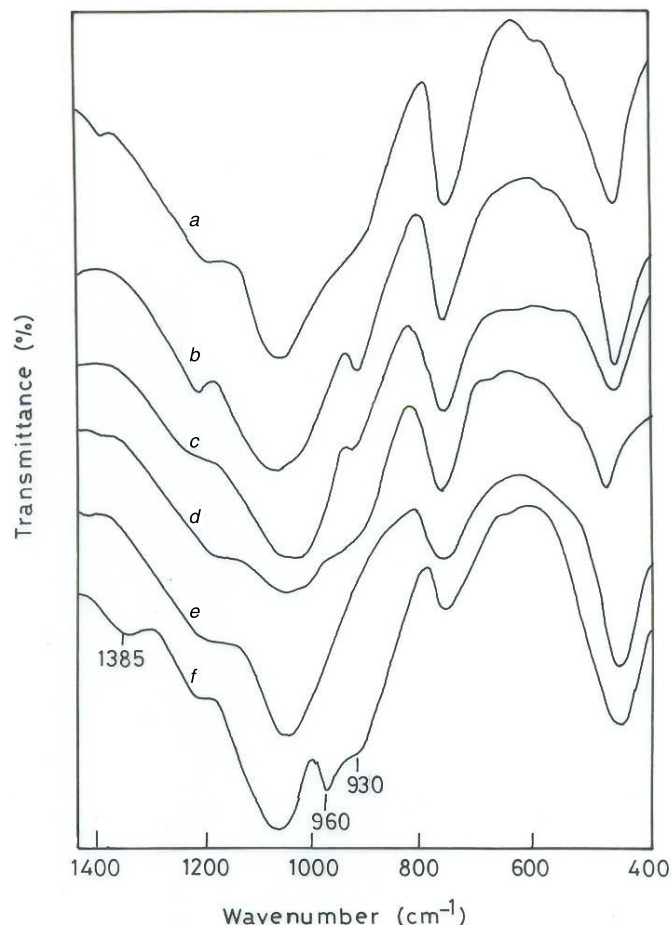


Samples B-1, B-2, B-3, B-4, and A-1 have a specific surface area of 920, 905, 935, 940, and 950 $\text{m}^2 \text{g}^{-1}$, respectively, and exhibit type IV N_2 adsorption isotherms with the characteristic step at $P/P_0 = 0.4$ (Fig. 3). This further confirms the mesoporous nature of the samples (45, 46). The average pore diameters and specific pore volume for the B-MCM-41 samples are presented in Table 1. The average pore diameters decrease slightly with increasing B content of the sample. This may be because of the nature of the synthesis mixture, perhaps a salt effect.

Infrared spectroscopy of B-MCM-41

The IR spectra of the synthesized B-1, B-2, B-3, and B-4 samples exhibit a series of bands in the 1600–250 cm^{-1} region, which are characteristic of the SiO_2 tetrahedron unit and its modification by the introduction of boron into the framework (Fig. 4). The location of boron in the synthesized samples B-1 to B-4 is confirmed from the presence of an IR band at 930 cm^{-1} , which is characteristic of tetra-coordinated boron in the MCM-41 framework (15). The intensity of this peak decreases as we go along from curves b to e in Fig. 4, and their decreasing trend is attributed to a decrease of boron content in the framework. The IR spectra of the Na-form and H-form of the typical sample B-1 are also shown in Fig. 4. The sample in its Na-form and dehydrated

Fig. 4. FT-IR spectra of the synthesized Al-MCM-41 and B-MCM-41 samples: (a) A-1; (b) B-1; (c) B-2; (d) B-3; (e) B-4; (f) H-form of B-1.

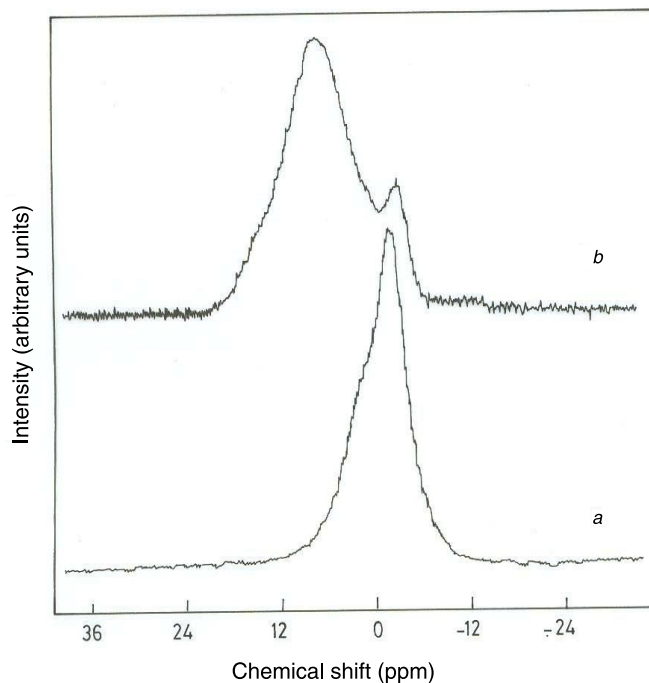


H-form exhibits weak bands at 930 and 1385 cm^{-1} , respectively, which are characteristic of tetra-coordinated boron and tri-coordinated boron in the MCM-41 framework, respectively (15). The fall in the IR band at 930 cm^{-1} and the appearance of a band at 1385 cm^{-1} , observed on the conversion of the Na-form of the sample to the H-form, show that, during the conversion, tetra-coordinated boron is converted to tri-coordinated boron. This observation was reported for both microporous (47, 48) and mesoporous borosilicates (15). This study shows that the tetra-coordinated boron is stable when sodium is counterbalancing the framework negative charge but unstable in the hydrogen form. The stability of these sites is caused by the formation of $\text{Na}^+\text{-B}(\text{OSi})_4^-$ units, which are coordinatively saturated and stable to hydrolysis (49). The H-forms of the B-MCM-41 samples also exhibit a new band at 960 cm^{-1} . Sayari et al. (13) and Ruiter et al. (49) assigned this band to the Si-OH groups in the silanol nests.

^{11}B -MAS NMR spectroscopy

Boron-11 MAS NMR spectra of a typical B-1 sample are shown in Fig. 5. The synthesized sample has one signal at -2.3 ppm. A similar signal was reported earlier in studies dealing with boron-modified MCM-41 and is assigned to B

Fig. 5. ^{11}B -MAS NMR spectra of B-1: (a) synthesized; (b) H-form.



in the framework tetrahedral coordination (17–20). The ^{11}B -MAS NMR spectrum of dehydrated, protonated B-MCM-41 reveals that most of the tetrahedral-coordinated boron has undergone a change in coordination. In addition to a small signal at -2.3 ppm, a very broad signal appears, which is typical for trigonal boron species in the MCM-41 framework (17–20). The FT-IR studies also support these findings.

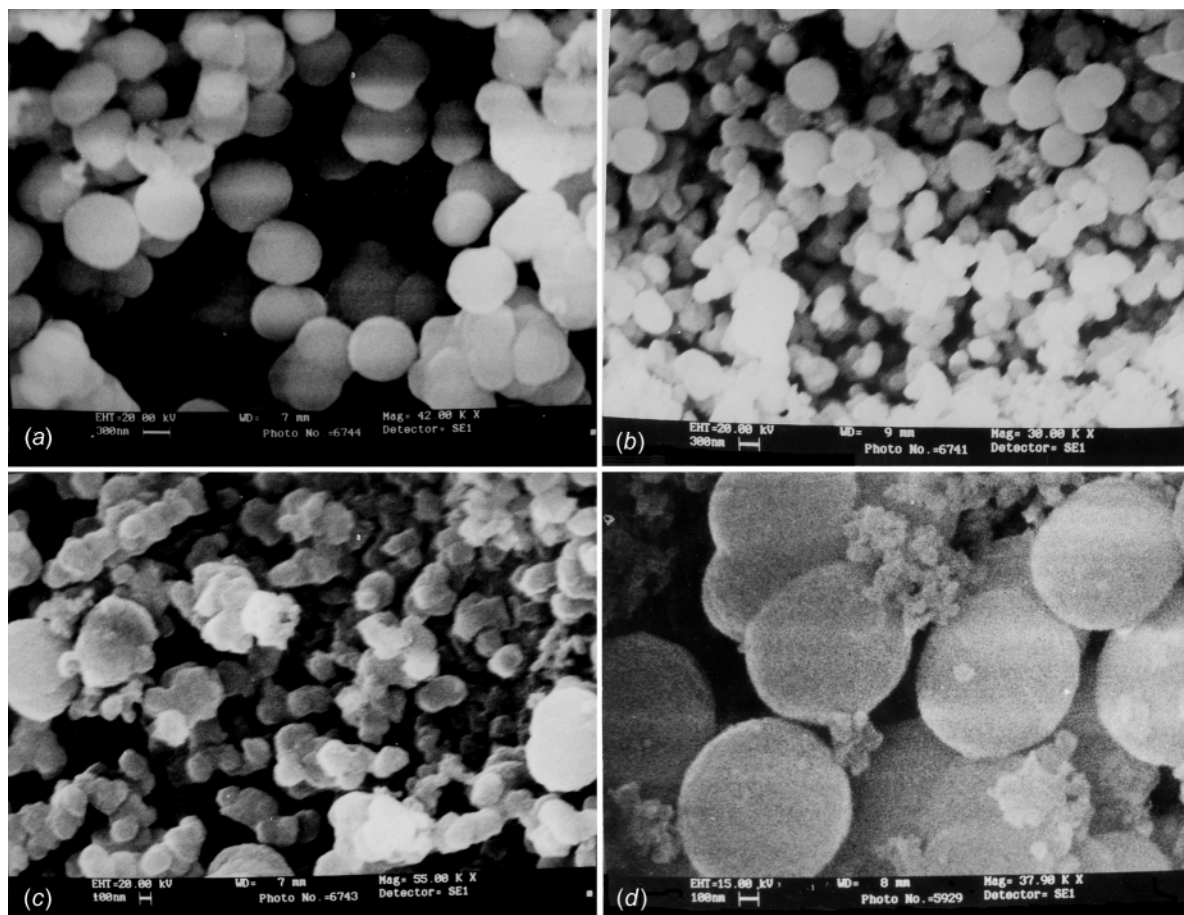
Scanning electron microscopy

Figure 6 represents the set of scanning electron micrographs of the B-MCM-41 samples. All B-MCM-41 samples have spherical particles. The size of these spheres is in the 500–1000 nm range. Small particles with size 100–300 nm with no distinct morphology also coexist with the spheres in all the samples. Among the samples, the change in morphology is small, and that change is only in size and not in the shape of the spheres.

Chemical composition

The molar compositions of the synthesized samples are shown in Table 2. The number of moles of Na_2O is lower than that of B_2O_3 , suggesting that not only Na^+ ions but also cetyltrimethylammonium cations are involved in neutralizing the negative charges of the framework. Chemical analysis shows that boron is released from the MCM-41 framework during (i) thermal decomposition of the template and (ii) thermal conversion of the NH_4 form to the H-form.

In each of the above-mentioned processes, the released boron was found to come out as H_3BO_3 and to stay as the extra framework material and was extracted out of the channels by washing with distilled water at room temperature. The $\text{SiO}_2\text{:B}_2\text{O}_3$ ratio of the washed samples was analyzed by

Fig. 6. Scanning electron micrographs of B-MCM-41: (a) B-1; (b) B-2; (c) B-3; (d) B-4.**Table 2.** Molar compositions of synthesized B-MCM-41 samples and % deboronation (β) of B-MCM-41 samples.

Sample	Synthesized samples (moles per mole B ₂ O ₃)				Deboronation (β) of B-MCM-41 (%)		
	SiO ₂	B ₂ O ₃	Na ₂ O	CTAB	I ^a	II ^b	Total
B-1	50	1	0.62	2.1	21.5	23.2	44.7
B-2	84	1	0.59	1.9	18.0	21.4	39.4
B-3	145	1	0.60	2.0	15.2	17.7	32.9
B-4	270	1	0.68	2.3	13.3	14.3	27.6

^aDeboronation during removal of template molecules.

^bDeboronation during thermal decomposition of the NH₄ form of the sample.

chemical analysis. The extent of boron released is expressed in terms of % deboronation (β) and is given in Table 2.

$$\beta = (1 - n_{\text{syn}}/n) \times 100$$

where n_{syn} and n denote the molar SiO₂:B₂O₃ ratio of the synthesized B-MCM-41 and that of the modified B-MCM-41, respectively. Table 2 shows that the deboronation level (β) decreases with an increase of the SiO₂:B₂O₃ ratio in the samples. This leads to the conclusion that the more boron is found in the MCM-41 framework, the weaker it is bound, and it is more likely that it is released during heat treatment.

FT-IR spectra of chemisorbed pyridine

Figure 7 depicts the FT-IR spectra of pyridine adsorbed on a B-1 sample in the region 1600–1400 cm⁻¹. The sample exhibits IR bands at 1595, 1545, and 1445 cm⁻¹. The bands at 1595 and 1445 cm⁻¹ are characteristic of physisorbed pyridine and hydrogen-bonded pyridine, respectively (15). The weak band at 1545 cm⁻¹ is characteristic of Brønsted acid sites (15). The thermal stability of pyridine sorbed on the catalyst was measured by increasing the desorption temperature from 100 to 250 °C. These bands are decreased sharply upon evacuation at elevated temperatures and disappear at 250 °C. This shows that B-MCM-41 possesses only weak and mild acid sites.

TPDA of B-MCM-41 and Al-MCM-41

TPDA spectra of Al-MCM-41 and B-MCM-41 samples are shown in Fig. 8. The TPDA spectra of Al-MCM-41 exhibit three maxima, viz. at ca. 167, 340, and 500 °C. The low-temperature peak is caused by desorption of ammonia from weak Brønsted and Lewis acid sites (50). The weak Brønsted acid sites appear as a result of surface hydroxyl groups, whereas the structural weak Lewis acid sites may arise from tricoordinated metal ion in the framework (51). The medium-temperature peak at 340 °C is assigned to weak- to medium-acidic Brønsted sites. Such sites are well known from medium-pore zeolites (52) and have been detected in substituted MCM-48 (53). The high-temperature signal is caused by ammonia desorbed from strong Lewis

Fig. 7. FT-IR spectra of pyridine adsorbed on B-1 at desorption temperatures of (a) 100, (b) 150, (c) 200, and (d) 250 °C.

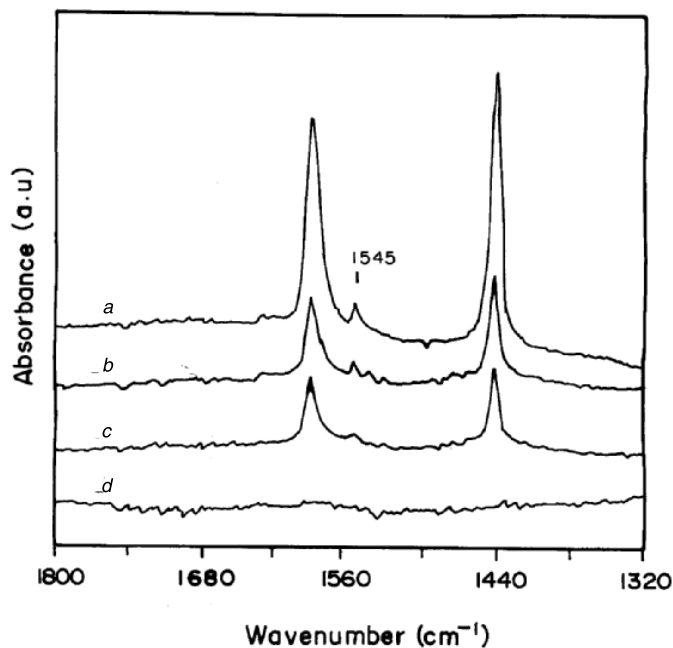
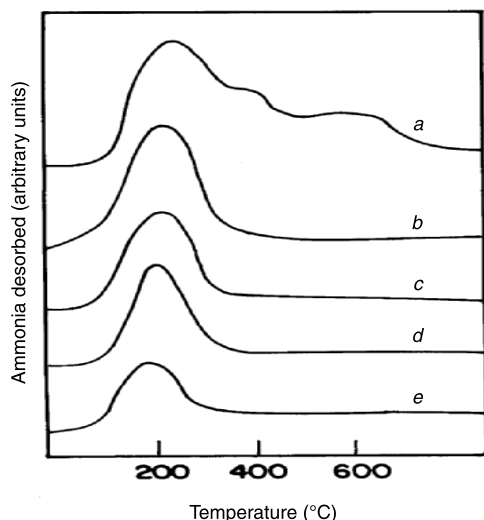


Fig. 8. TPDA of Al-MCM-41 and B-MCM-41: (a) A-1; (b) B-1; (c) B-2; (d) B-3; (e) B-4.



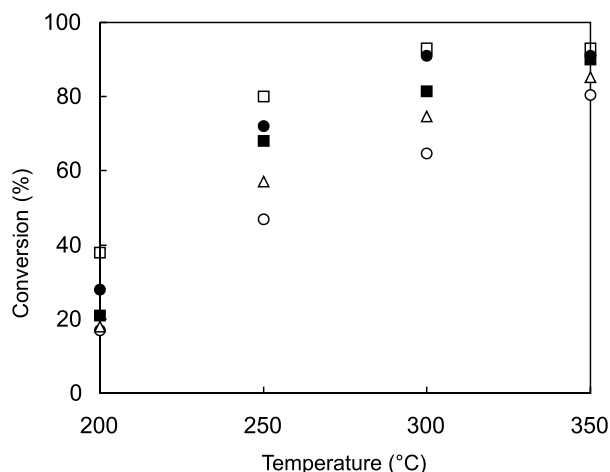
acid sites (53). The concentration of strong Lewis sites points to the dispersion of the extra framework aluminum species in the channels of MCM-41.

The major deviations observed in the TPD spectra on isomorphous substitution of B for Al are the absence of medium- and high-temperature signals and the presence of only low-temperature signals corresponding to weak Lewis and Brønsted acid sites. This study shows that boron substitution in the MCM-41 framework results in only weak acid sites like those of B-ZSM-5 samples (54, 55).

Catalytic studies

Isomerization of 1-hexene was carried out in the temperature range 200–350 °C and at a liquid hourly space velocity

Fig. 9. 1-Hexene conversion (wt %) at different temperatures, LHSV = 3 h⁻¹: (●) B-1; (■) B-2; (△) B-3; (○) B-4; (□) A-1.



(LHSV) of 3 h⁻¹ over the H-form of catalysts B-1 to B-4 and A-1, all of which were activated at 500 °C. LHSV is the ratio of the weight of the liquid feed per hour (g h⁻¹) and the weight of the catalyst (g). The conversion of 1-hexene at different temperatures is presented in Fig. 9. At any given temperature, a decreasing trend of isomerization was observed with increasing SiO₂:B₂O₃ ratio of the catalyst, viz. 91%, 81.5%, 74.6%, and 64.7% conversions were obtained over catalysts B-1, B-2, B-3, and B-4, respectively, at 300 °C. The decrease in conversion is attributed to the decrease in the number of acid sites present in the catalyst as the SiO₂:B₂O₃ ratio increases. At all temperatures, higher conversion was obtained over the A-1 catalyst than over boron-substituted catalysts because of the presence of strong Brønsted acidic sites associated with the presence of Al³⁺. As the temperature increased from 200 °C, the conversion of 1-hexene was found to increase for all the catalysts, and a maximum conversion (93%) of 1-hexene over the A-1 catalyst was observed at 300 °C, whereas for the B-1, B-2, B-3, and B-4 catalysts, the maximum conversions of 91%, 90%, 85.2%, and 80.5% were observed at 350 °C. Si-MCM-41 was also tested under similar conditions and was found to have no catalytic activity in the temperature range 200–350 °C.

Table 3 shows the product selectivity of 1-hexene isomerization at the following temperatures: 200, 250, 300, and 350 °C. The reaction products shown in the above-mentioned table are formed generally via double-bond shift, *cis*–*trans* isomerization, and skeletal rearrangement. The major isomerization products *trans*-2-hexene (*t*-2H), *cis*-2-hexene (*c*-2H), and (*cis*+*trans*)-3-hexene ((*c*+*t*)-3H) are formed by a 1–2 double-bond shift. For instance, at 300 °C *trans*-2-hexene, *cis*-2-hexene, and (*cis*+*trans*)-3-hexene constitute 95.9% of the total, from 88% conversion on B-1. This is comparable to the 94.75% double-bond shift at 54% conversion reported by Ko and Wojciechowski (38) on an HY catalyst at 200 °C and to that of 95% on ZSM-5 at 52% conversion reported by Abbot et al. (39) at 280 °C.

The increase of temperature from 200 to 350 °C shows a decrease in the selectivity of 2-hexene with a simultaneous increase in selectivity of 3-hexene. However, between the 2-hexenes, the selectivity of *trans*-2-hexene is not affected as

Table 3. Selectivity of 1-hexene isomerization products.

Product	Selectivity of products over different catalysts (wt %)				
	A-1	B-1	B-2	B-3	B-4
Selectivity of products at 200 °C					
t-2H	51.9	47.2	48	48.6	49
c-2H	38.1	44.6	45.4	46.4	47
(t+c)-3H	10	8.2	6.6	5	4
Selectivity of products at 250 °C					
t-2H	48.4	49	50	50.3	53.8
c-2H	29.9	32	33	34.2	36.2
(t+c)-3H	18.1	17	16	15.5	10.2
2M2P	3.6	2	1	—	—
Selectivity of products at 300 °C					
t-2H	41.8	48	49	50	51
c-2H	20.2	28	30	32	33.4
(t+c)-3H	15.5	19.9	17.8	16.1	14
2M2P	9.9	2.7	3.2	1.9	1.6
3M2P	4	1.3	—	—	—
4M2P	2.2	—	—	—	—
2M1P	3.2	—	—	—	—
3M1P	2.2	—	—	—	—
Selectivity of products at 350 °C					
t-2H	35.5	44.5	46.4	47.8	49.5
c-2H	13.8	24.7	28.1	29.9	31.5
(t+c)-3H	13.5	21.3	19.1	19.5	17
2M2P	13.4	5.8	4.2	2.8	2
3M2P	9.3	2.6	2.2	—	—
4M2P	3.8	1.1	—	—	—
2M1P	7.5	—	—	—	—
3M1P	3.2	—	—	—	—

Note: t-2H, *trans*-2-hexene; c-2H, *cis*-2-hexene; (c+t)-3H, (*cis*+*trans*)-3-hexene; 2M2P, 2-methyl-2-pentene; 3M2P, 3-methyl-2-pentene; 4M2P, 4-methyl-2-pentene; 2M1P, 2-methyl-1-pentene; 3M1P, 3-methyl-1-pentene.

much by temperature as that of *cis*-2-hexene. Over the A-1 catalyst, the selectivities of both t-2H and c-2H are affected similarly by a raise in temperature. Similarly, at any fixed temperature studied, an increase of boron content in the catalyst increases the selectivity of 3-hexenes and decreases that of 2-hexenes.

Skeletal isomerization products in considerable quantity are found to form on the A-1 catalyst as secondary products from 250 °C onwards, and they increase with an increase in temperature. They are 2-methyl-2-pentene (2M2P), 3-methyl-2-pentene (3M2P), 4-methyl-2-pentene (4M2P), 2-methyl-1-pentene (2M1P), and 3-methyl-1-pentene (3M1P). Among them, 2M2P and 3M2P are the major ones. At 250 °C and above, only small amounts of 2M2P and 3M2P are formed with each of the boron catalysts, as compared to the aluminum catalyst. For example, at 300 °C, the maximum skeletal isomerization product formed over B-1 amounts to 4.0% compared to 21.5% over A-1. Similarly, at any fixed temperature studied, selectivity of the skeletal isomerization products was found to increase with an increase of the boron content of the catalysts.

The mechanism of the reported double-bond shift (30) involves interaction of 1-hexene with the acid sites of the cata-

lysts, leading to the formation of the C₆ carbenium ion. The carbenium ion can undergo deprotonation, hydrogen shift, cyclization, or oligomerization. The formation of 2-hexene is attributed to deprotonation and that of 3-hexene to a hydrogen shift. The large difference in the selectivity of 2-hexenes from that of 3-hexenes suggests that the rate of deprotonation from the carbenium ion is much faster than that of the hydrogen transfer from the C₆ carbenium ion. Skeletal isomerization products are formed by a sequence of hydrogen and methyl shifts. These are energy-demanding steps and, hence, register low selectivity over boron-substituted catalysts compared with the aluminum-substituted catalyst.

Ratios of selectivity of double-bond shift products of hexene (c-2H:t-2H and (c+t)-2H:(c+t)-3H) at four different temperatures over all the catalysts are shown in Table 4. The thermodynamic equilibrium ratios 0.39, 0.44, and 0.44 have been reported by Abbot et al. (39) for c-2H to t-2H at 200, 250, and 280 °C, respectively. Any different ratio of c-2H to t-2H than the above-mentioned ones is a clear indication that the reaction is kinetically controlled. Thus, ratios in Table 4 show that the reaction is kinetically controlled, with higher relative rates of production of *cis* isomers at all temperatures. Similar preferential formation of *cis* isomers has been reported by Abbot and Wojciechowski (40) over ZSM-5 and by Ko and Wojciechowski (38) over HY catalysts. We also observed and reported a similar result over B-ZSM-5 catalysts (26). The excess of the *cis* isomer with respect to the *cis:trans* equilibrium ratio is attributed to (i) steric effects on the C₆ carbenium ion leading to its preferential formation of c-2H (45) and (ii) the formation of a more stable intermediate π complex between the *cis* isomer and the proton on the Brønsted sites (38).

It is apparent from Table 4 that the c-2H:t-2H ratio decreases with an increase of temperature with all the catalysts. Similar results have been reported over the ZSM-5 catalyst (39). We have already reported the 1-hexene isomerization on B-ZSM-5 catalysts (26). The c-2H:t-2H ratio obtained with the B-ZSM-5 samples (26) is significantly lower than with the B-MCM-41 samples under similar conditions. This is probably a result of different pore structures and dimensions in the two molecular sieves. The elliptical channels in B-ZSM-5 have diameters (5 to 6 Å) in a range approaching the kinetic diameters of straight-chain olefins (4.3 Å). This property has led to a wide interest in the reactions (which are said to control shape selectivity) of hydrocarbons in this microporous molecular sieve. The reason for *cis:trans* ratios closer to equilibrium in B-ZSM-5 is associated with the initial spatial requirements of the transition state followed by equilibration encouraged by diffusional limitations. There is a high probability that a particular 2-hexene molecule, once formed, will undergo repeated collision with the channel walls before escaping from ZSM-5 channels. The above-mentioned equilibration is absent in B-MCM-41 because of the *meso* pore size, and it shows higher c-2H:t-2H ratios in relation to those of the B-ZSM-5 catalysts.

From the percentage of selectivity of c-2H, t-2H, and (c+t)-3H, values of the 2-hexenes:3-hexenes ratio, (c+t)-2H:(c+t)-3H, have been calculated and are presented in Table 4. At all temperatures, as the SiO₂:B₂O₃ ratio of catalysts

Table 4. Ratio of selectivity for isomerization of 1-hexene on the A-1 and B-1 to B-4 catalysts.

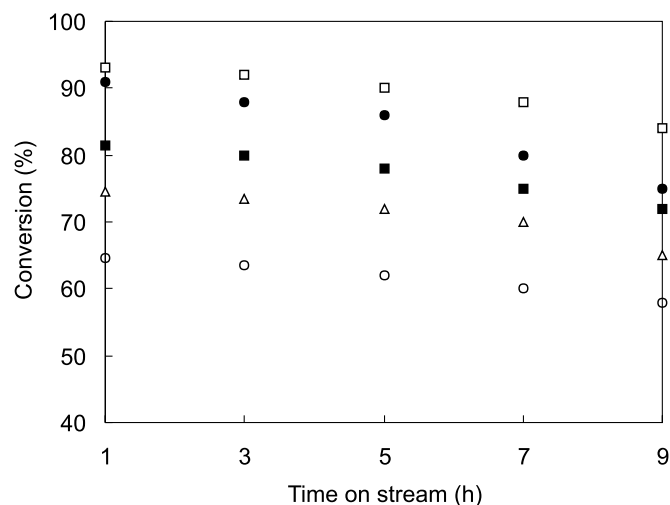
Catalyst	c-2H:t-2H				(c+t)-2H:(c+t)-3H			
	200 °C	250 °C	300 °C	350 °C	200 °C	250 °C	300 °C	350 °C
A-1	0.73	0.62	0.48	0.39	9	4.3	4	3.6
B-1	0.94	0.65	0.58	0.56	11.2	4.8	3.9	3.2
B-2	0.95	0.66	0.61	0.6	14.1	5.2	4.4	3.7
B-3	0.95	0.68	0.64	0.63	19	5.5	4.9	4.1
B-4	0.96	0.69	0.65	0.64	24	8.8	6	4.8
B-ZSM-5 ^a	0.62	0.42	0.41	0.34	12.3	7.6	4.6	3.8
B-ZSM-5 ^b	0.64	0.44	0.44	0.37	15.6	10.7	7.2	4.7

^aSiO₂:B₂O₃ ratio = 180.^bSiO₂:B₂O₃ ratio = 350 (from ref. 26).

decreases, the (c+t)-2H:(c+t)-3H ratio decreases. This is ascribed to the increase in the number of acid sites of the catalyst with an increase of boron content in the framework, which in turn increases the rate of hydrogen shift from the 3- to the 2-carbon and enhances the formation of 3-hexene. Similarly, an increase of temperature from 200 to 350 °C increases the rate of hydrogen shift to form 3-hexene. A similar observation was also reported (39) over the ZSM-5 catalyst in the 1-hexene isomerization with an increase of reaction temperature.

The conversions of 1-hexene vs. time on stream over all the catalysts at 300 °C are shown in Fig. 10. The conversion of 1-hexene decreases steadily over all the catalysts with increasing time on stream, though the actual decrease is different for different catalysts. This is mainly because catalysts lose their activity steadily with time on stream. The activity loss is attributed to coke formation, which increases with time on stream, thereby poisoning the active acidic sites. The wt % coke formed is 7.4%, 6.9%, 6.6%, 6.1%, and 4.0% on the B-1, B-2, B-3, B-4, and A-1 catalysts, respectively, at the end of 9 h at 300 °C. It was observed that an increase of boron content in the framework slightly increases the coking and aging during time on stream. The amount of coke accumulation on boron-containing catalysts is greater than that on the corresponding aluminum-containing catalyst. Cornaro and Wojciechowski (30) also observed a greater amount of coke accumulation over the B-ZSM-5 catalyst than the Al-ZSM-5 catalyst in the 1-hexene isomerization. The difference in the coke content is a result of the difference in the acidity of the catalysts. Al-MCM-41 can crack off the precoke oligomer in the process of coke hardening because of the presence of a greater number of strong acidic sites, thus resulting in a lesser amount of coke. The boron catalysts, which have a mild acidity, are apparently not able to crack the precoke (26, 30) and, hence, accumulate a greater amount of coke.

FT-IR spectra of coke-deposited catalysts show the prominent IR band in the C-H deformation region around 1600 cm⁻¹ (this figure is not shown). Eberly (56) ascribed this band to highly unsaturated carbonaceous residues, most likely adsorbed olefins. Abbot et al. (39) also observed the presence of mainly adsorbed olefins in the coke deposit on the ZSM-5 catalyst in the 1-hexene isomerization in the temperature range 200–350 °C. A TGA study of the coke formed on catalysts shows the formation of only soft coke molecules (TGA weight loss occurs between 300 and

Fig. 10. Effect of time on stream on 1-hexene conversion at 300 °C, LHSV = 3 h⁻¹: (●) B-1; (■) B-2; (△) B-3; (○) B-4; (□) A-1.

500 °C) on the B-MCM-41 and the Al-MCM-41 catalysts in the above-mentioned reaction temperature range.

Conclusion

The B-MCM-41 samples, with differing amounts of boron in the framework, were synthesized by a hydrothermal method using ES-40. Evidence for the presence of B in the silica network of MCM-41 was obtained by different characterization techniques. In the synthesized samples, boron was present in the four-coordinated state. Calcination and further conversion into the H-form converted a significant part of the boron into a three-coordinated state. The % deboronation of B-MCM-41 was found to be dependent on the concentration of boron in the silicate framework. Investigation of the acidity of B-MCM-41 revealed that the materials have only a weak acidity and a lower acidity than that of Al-MCM-41. The catalytic effect of framework boron, explored by means of 1-hexene isomerization, reveals that the extent of 1-hexene conversion changes with boron content and, hence, the acidity of the catalysts. The isomorphous substitution of B for Al in the MCM-41 framework changes both the conversion of 1-hexene and the selectivity of the products. The selectivity of the double-bond shift products is enhanced with the substitution of B for Al in the MCM-41 framework.

References

1. C.T. Kresge, M.E. Leonowicz, W.J. Roth, and J.C. Vartulli. U.S. Patent 5 098 684, 1992; U.S. Patent 5 102 643, 1992.
2. C.T. Kresge, M.E. Leonowicz, W.J. Roth, J.C. Vartulli, and J.S. Beck. *Nature (London)*, **359**, 710 (1992).
3. J.S. Beek, J.C. Bartuli, W.J. Roth, M.E. Leonowicz, C.T. Kresge, K.D. Schmitt, C.T.-W. Chu, D.H. Olson, E.W. Sheppard, S.B. Mccullen, J.B. Higgins, and J.L. Schlenker. *J. Am. Chem. Soc.* **114**, 10 834 (1992).
4. A. Corma, V. Fornes, M.T. Navarro, and J. Perez-Pariente. *J. Catal.* **148**, 569 (1994).
5. R. Schmidt, D. Akporiaye, M. Stocker, and O.H. Ellested. *J. Chem. Soc. Chem. Commun.* 1493 (1994).
6. C.Y. Chen, H.X. Li, and M.E. Davis. *Microporous Mater.* **2**, 17 (1993).
7. C.Y. Chen, S.L. Burkett, H.X. Li, and M.E. Davis. *Microporous Mater.* **2**, 27 (1993).
8. Z. Luan, C-F. Cheng, W. Zhou, J. Klinowski, J.A. Sousa-Goncalves, and L.F. Gladden. *J. Phys. Chem.* **99**, 1018 (1995).
9. P.T. Tanev, M. Chibwe, and T.J. Pinnavaia. *Nature (London)*, **368**, 321 (1994).
10. C.G. Wu and T. Bein. *Science (Washington, D.C.)*, **264**, 1757 (1994).
11. C-F. Cheng, H. He, W. Zhou, and J. Klinowski. *J. Phys. Chem.* **100**, 390 (1996).
12. K.M. Reddy, I. Moudrakovski, and A. Sayari. *J. Chem. Soc. Chem. Commun.* 1059 (1994).
13. A. Sayari, K.M. Reddy, and I. Moudrakovski. *Stud. Surf. Sci. Catal.* **98**, 19 (1995).
14. U. Oberhagemann, I. Topalovic, B. Marler, and H. Gies. *Stud. Surf. Sci. Catal.* **98**, 17 (1995).
15. D. Trong On, P.N. Joshi, G. Lemay, and S. Kaliaguine. *Stud. Surf. Sci. Catal.* **97**, 543 (1995).
16. A. Sayari, C. Danumah, and I.L. Moudrakovski. *Chem. Mater.* **7**, 813 (1995).
17. A. Sayari, I. Moudrakovski, C. Danumah, C.I. Ratcliffe, J.A. Ripmeester, and K.F. Preston. *J. Phys. Chem.* **99**, 16 373 (1995).
18. D. Trong On, P.N. Joshi, and S. Kaliaguine. *J. Phys. Chem.* **100**, 6743 (1996).
19. S. Liu, H. He, Z. Luan, and J. Klinowski. *J. Chem. Soc. Faraday Trans.* **92**, 2011 (1996).
20. U. Oberhagemann, I. Kinski, I. Dierdorf, B. Marler, and H. Gies. *J. Non-Cryst. Solids*, **145**, 197 (1996).
21. S. Gontier and A. Tuel. *Stud. Surf. Sci. Catal.* **105**, 29 (1997).
22. U. Oberhagemann, M. Jeschke, and H. Papp. *Microporous Mesoporous Mater.* **33**, 165 (1999).
23. Z.Y. Yuan, Q. Luo, J.Q. Liu, T.H. Chen, J.Z. Wang, and H.X. Li. *Microporous Mesoporous Mater.* **42**, 289 (2001).
24. M.S. Rigutto, R. de Ruiter, J.P.M. Niederer, and H. Van Bekkum. *Stud. Surf. Sci. Catal.* **84**, 2245 (1994).
25. C.B. Dartt and M.E. Davis. *Appl. Catal.* **143**, 53 (1996).
26. V. Sundaramurthy and N. Lingappan. *J. Mol. Catal.* **160**, 367 (2000).
27. D.P. Sabde, S.G. Hegde, and M.K. Dongare. *J. Mater. Chem.* **10**, 1365 (2000).
28. J. Mrowiec-Bialon and A.B. Jarzebski. *Langmuir*, **17**, 626 (2001).
29. R. Fischer, W. Holderich, W.D. Mross, and H.M. Weitz. *European Patent* 0 167 021, 1986.
30. U. Cornaro and B.W. Wojciechowski. *J. Catal.* **120**, 182 (1989).
31. W. Holderich, F. Merger, W.D. Mross, and G. Fouguet. *European Patent* 0 162 385, 1985.
32. L.B. Pierella, O.A. Anunziata, and O.A. Orío. *Lat. Am. Appl. Res.* **25**, 223 (1995).
33. J. Roseler, G. Heitmann, and W.F. Holderich. *Appl. Catal.* **144**, 319 (1996).
34. E. Dumitriu, D. Trong On, and S. Kaliaguine. *J. Catal.* **170**, 150 (1997).
35. H. Pines and W.O. Haag. *J. Am. Chem. Soc.* **82**, 2471 (1960).
36. D.M. Brouwer. *J. Catal.* **1**, 22 (1962).
37. P.B. West, G.L. Haller, and R.L. Burwell. *J. Catal.* **29**, 486 (1973).
38. A.N. Ko and B.W. Wojciechowski. *Int. J. Chem. Kinet.* **15**, 1249 (1983).
39. J. Abbot, A. Corma, and B.W. Wojciechowski. *J. Catal.* **92**, 398 (1985).
40. J. Abbot and B.W. Wojciechowski. *Can. J. Chem. Eng.* **60**, 622 (1985).
41. G. Gati and G. Resofszki. *Kem. Kozl.* **72**, 86 (1991).
42. Z. Paal, M. Raeth, B. Brose, and W. Gomber. *React. Kinet. Catal. Lett.* **47**, 43 (1992).
43. D. Zhiping and X. Changqing. *Riyoung Huaxue Gongye*, **20**, 12 (1996).
44. F.A. Twaiq, N.A.M. Zabidi, and S. Bhatia. *Ind. Eng. Chem. Res.* **38**, 3230 (1999).
45. P.J. Branton, P.G. Hall, and K.S.W. Sing. *J. Chem. Soc. Chem. Commun.* 1257 (1993).
46. D. Franke, G. Schulz-Ekloff, and J. Rathousky. *J. Chem. Soc. Chem. Commun.* 724 (1993).
47. G. Coudurier, A. Auroux, J.C. Vedrine, R.D. Farlee, L. Abrams, and R.D. Shannon. *J. Catal.* **108**, 1 (1987).
48. D. Trong On, M.P. Kapoor, L. Bonneviot, S. Kaliaguine, and Z. Gabelica. *J. Chem. Soc. Faraday Trans. 1*, **92**, 1031 (1996).
49. R.D. Ruiter, K. Pamin, A.P.M. Kentgens, J.C. Jansen, and H. Van Bekkum. *Zeolites*, **13**, 611 (1993).
50. H. Kosslick, G. Lischke, B. Parltitz, W. Storek, and R. Fricke. *Appl. Catal.* **184**, 49 (1999).
51. S.K. Badamali, A. Sakthivel, and P. Selvam. *Catal. Lett.* **65**, 153 (2000).
52. H.G. Karge, V. Dondur, and J. Weitkamp. *J. Phys. Chem.* **95**, 283 (1991).
53. H. Kosslick, G. Lischke, H. Landmesser, B. Parltitz, W. Storek, and R. Fricke. *J. Catal.* **176**, 102 (1998).
54. K.F.M.G.J. Scholle, A.P.M. Kentgens, W.S. Veeman, P. Frenken, and G.P.M. Van der Velden. *J. Phys. Chem.* **88**, 5 (1984).
55. M.W. Simon, S.S. Nam, W.-q. Xu, S.L. Suib, J.C. Edwards, and C.L. O'Young. *J. Phys. Chem.* **96**, 6381 (1992).
56. P.E. Eberly, Jr. *J. Phys. Chem.* **71**, 1717 (1967).